Supporting Information

Modulating the Electrocatalytic Performance of Palladium with the Electronic Metal–Support Interaction: A Case Study on Oxygen Evolution Reaction

Hongyang He,[†,#] Junxiang Chen,[§,#] Dafeng Zhang,[*,†,‡] Fang Li,[‡] Xin Chen,[†] Yumei Chen,[†] Linyan Bian,[†] Qiufen Wang,[†] Peigao Duan,[†] Zhenhai Wen,[*,§] and Xiaojun Lv[*,‡]

[†]Department of Energy and Chemical Engineering, College of Chemistry and Chemical Engineering, Henan Polytechnic University, Jiaozuo 454003, P. R. China

[‡]Key Laboratory of Photochemical Conversion and Optoelectronic Materials & CAS-HKU Joint Laboratory on New Materials, Technical Institute of Physics and Chemistry, Chinese Academy of Sciences, Beijing 100190, P.R. China

[§]CAS Key Laboratory of Design and Assembly of Functional Nanostructures, and Fujian Province Key Laboratory of Nanomaterials, Fujian Institute of Research on the Structure of Matter, Chinese Academy of Sciences, Fuzhou, 350002, P.R. China

*E-mail: dfzhang@hpu.edu.cn (D.F. Zhang); xjlv@mail.ipc.ac.cn (X.J. Lv); wen@fjirsm.ac.cn (Z.H. Wen)

[#]H.H and J.C. contributed equally.

1. Computational Method

1.1. Details of DFT

Spin-polarized DFT calculations were performed with periodic super-cells under the generalized gradient approximation (GGA) using the Perdew-Burke-Ernzerhof (PBE) functional for exchange-correlation and the ultrasoft pseudopotentials for nuclei and core electrons. The Kohn-Sham orbitals were expanded in a plane-wave basis set with a kinetic energy cutoff of 30 Ry and the charge-density cutoff of 300 Ry. The Fermi-surface effects has been treated by the smearing technique of Methfessel and Paxton, using a smearing parameter of 0.02 Ry. Periodically repeated two-layer slabs are modelled for both Fe_2O_3 (001) and PdO (001), each layer of Fe_2O_3 (001) and PdO (001) contain trilayer Fe_2O_3 and bilayer PdO units, respectively. The DFT-optimized equilibrium lattice constants are 4.95 Å and 3.04 Å for PdO and Fe_2O_3. For both slabs, the bottom one layer was fixed and the top layer was allowed to relax with the adsorbates during the calculations until the Cartesian force components acting on each atom were below 10^{-3} Ry/Bohr and the total energy converged to within 10^{-5} Ry. A supercell of (2×1) is used for both slabs. The Brillouin-zones were sampled with 1×2×1 and 3×2×1 k-point mesh for PdO (001) and Fe_2O_3 (001). The PWSCF codes contained in the Quantum ESPRESSO distribution[S1] were used to implement all of the calculations.

1.2. The Calculating of Chemical Potentials of Adsorbates.

For all the associated adsorbates, the O atoms are considered to follow their original positions in the crystals. The chemical potentials of adsorbates X* is calculated by the following expression:

$$\mu_{X^*} = E_{X^*\text{-slab}} - E_{\text{slab}} + ZPE_{X^*} - TS_{X^*} \quad \text{S1}$$

The $E_{X^*\text{-slab}}$ and E_{slab} are the DFT based total energies of slabs with and without the adsorbates X*. The *ZPE* and *TS* are the contributions from zero points and entropies of adsorbates, whose values are listed on Table S2. The OER follows the classical 4 proton coupled electron transfer (PCET) process[S2] that is written as:

$$H_2O(l) + * \rightarrow OH^* + H^+(aq) + e \quad \text{S2}$$

$$OH^* \rightarrow O^* + H^+(aq) + e \quad \text{S3}$$

$$O^* + H_2O \rightarrow OOH^* + H^+(aq) + e \quad \text{S4}$$

$$OOH^* \rightarrow O_2(g) + * \quad \text{S5}$$

The asterisk stands for the site on the surface of a certain catalyst. The free energies of $O_2(g)$ are calculated by the equilibrium of $O_2(g) + 4H^+(aq) + 4e \rightarrow 2H_2O(l)$ on 1.23 V to avoid the error of DFT energy caused by the high spin of O_2.[S3–S4] The free energy of $H^+(aq)$ is calculated by the $1/2H_2(g)$ on the basis of computational hydrogen electrode (CHE) method.[S5]

1.3. The Coordinating Number of Fe/Pd during OER

Similar to Ref. S6, the surface oxidation process is caused by the co-effects between H_2O and electron from electrode, which is the summation of reactions S1 and S2:

$$H_2O(l) + * \rightarrow O^* + 2H^+(aq) + 2e \quad \text{S6}$$

The O* formation energy ($\Delta\mu_{O^*}$) in Figure 6a is expressed as:

$$\Delta\mu_{O^*} = \mu_{O^*}(CN) - \mu^0_{O^*} \quad \text{S7}$$

where $\mu_{O^*}(CN)$ is the chemical potential of O* under a certain coordinating number (CN). $\mu^0_{O^*}$ is the chemical potential of O* that leads to the equilibrium of S6 on 1.5 V. 1.5 V was chosen for it is the most interesting potential of OER.

2. Supporting Figures

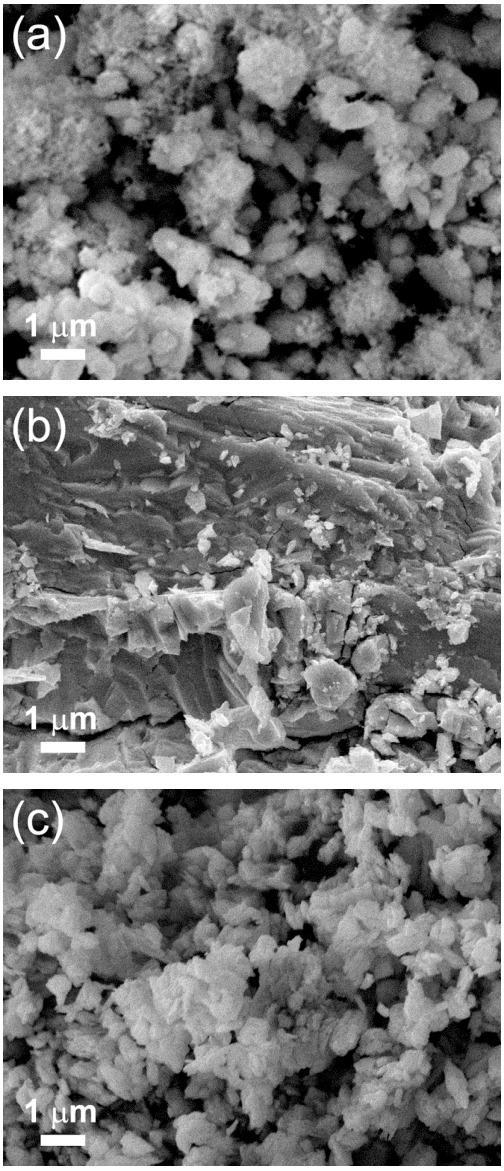

Figure S1. SEM images of the powdery metal oxides of (a) Fe_2O_3, (b) WO_3, and (c) MoO_3.

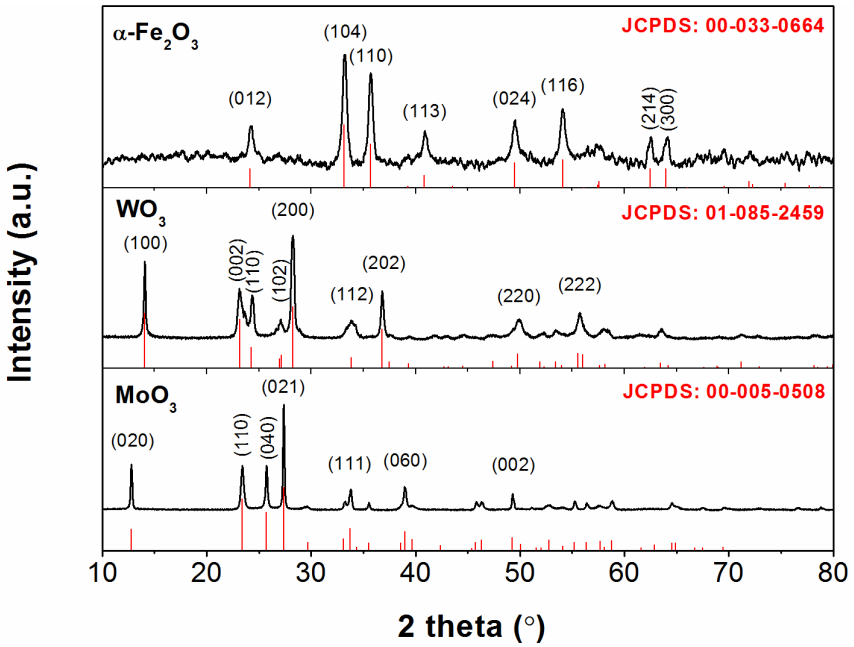

Figure S2. XRD patterns of the powdery α-Fe_2O_3, WO_3, and MoO_3.

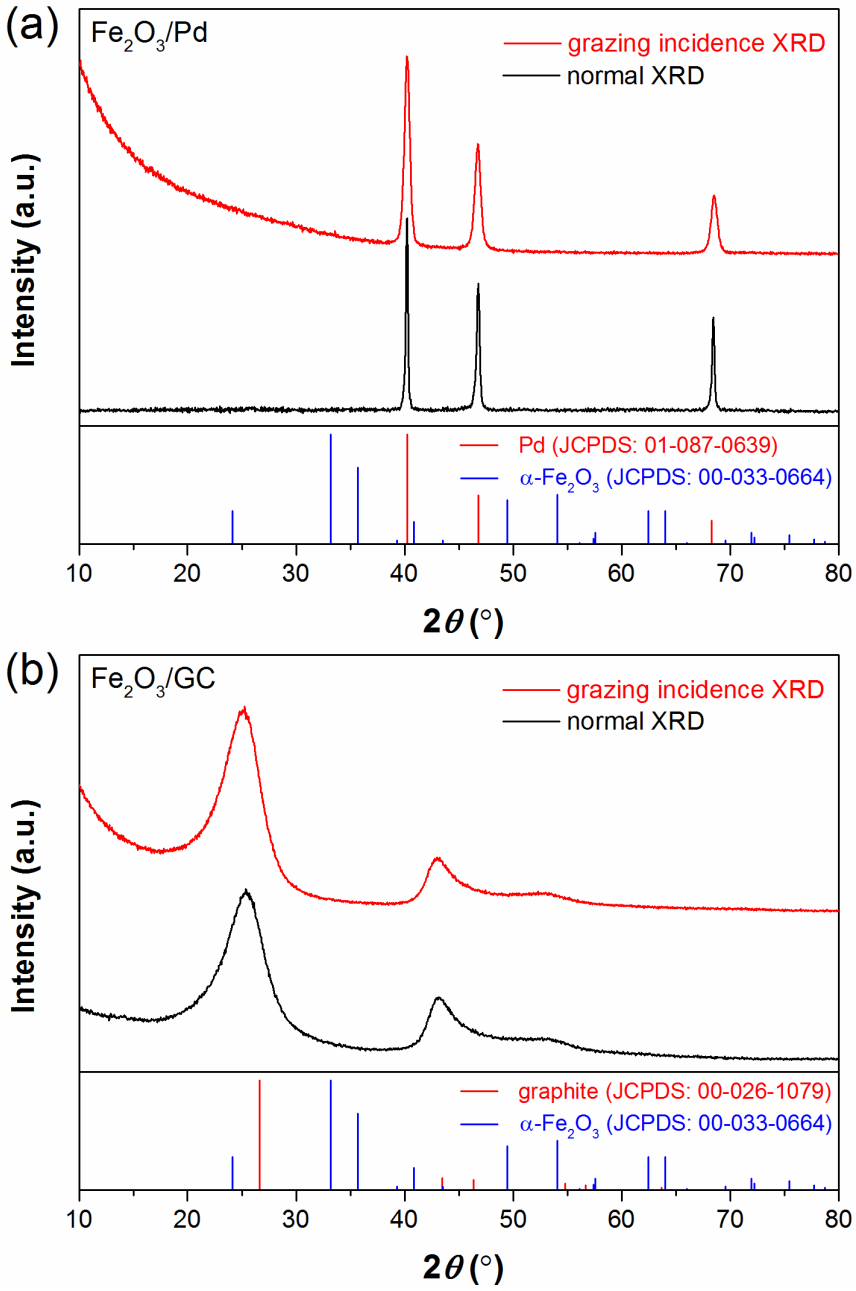

Figure S3. Normal powder XRD patterns (black lines) and grazing incidence XRD patterns (red lines) of (a) Fe_2O_3/Pd and (b) Fe_2O_3/GC catalysts.

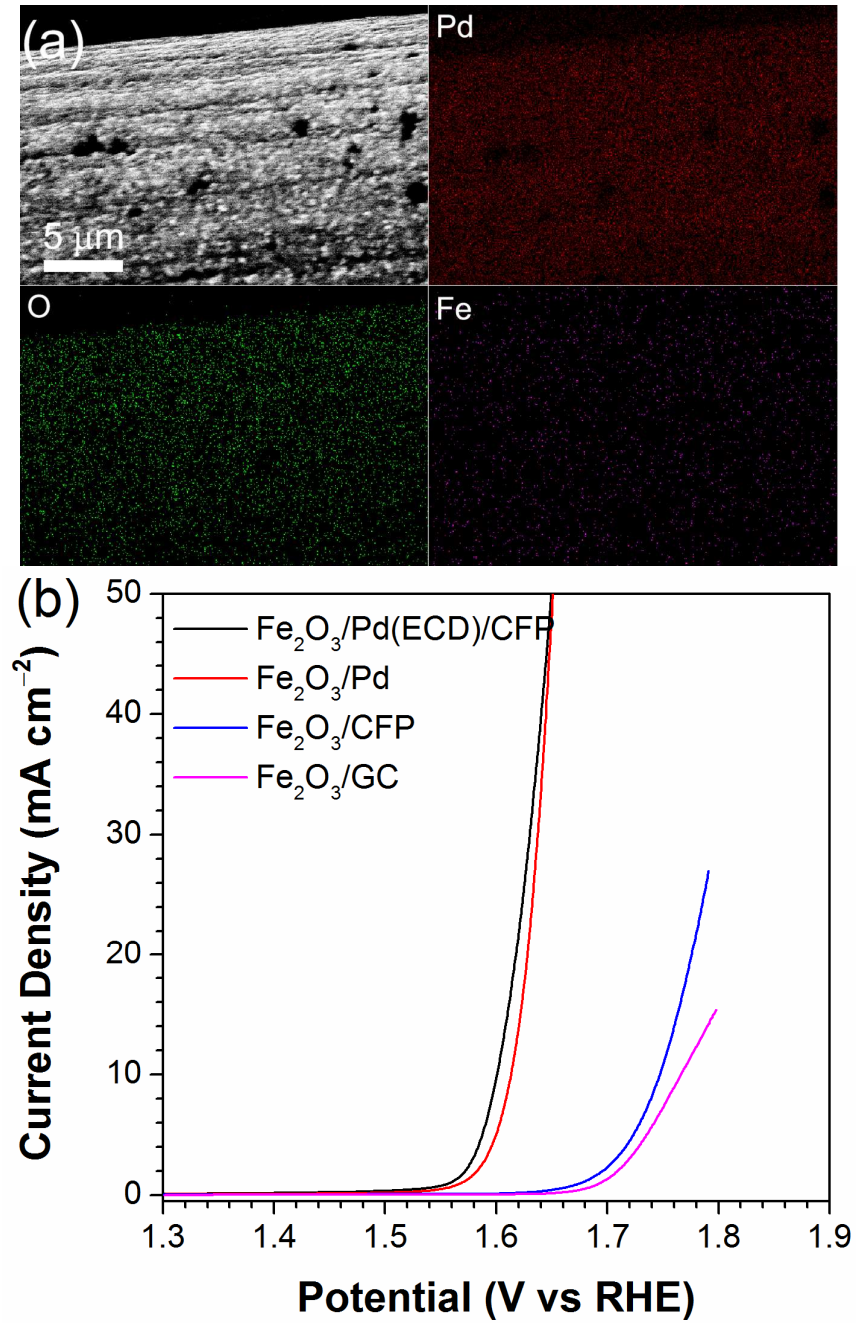

Figure S4. (a) Elemental mapping analysis of Fe_2O_3/Pd(ECD) on CFP. (b) OER electrocatalysis in 1 M KOH. *iR*-corrected LSV curves recorded at a scan rate of 10 mV s^{-1} on Fe_2O_3/Pd(ECD)/CFP, Fe_2O_3/Pd, Fe_2O_3/CFP, and Fe_2O_3/GC samples. The Pd(ECD) refers to the Pd film prepared by electrochemical deposition method.

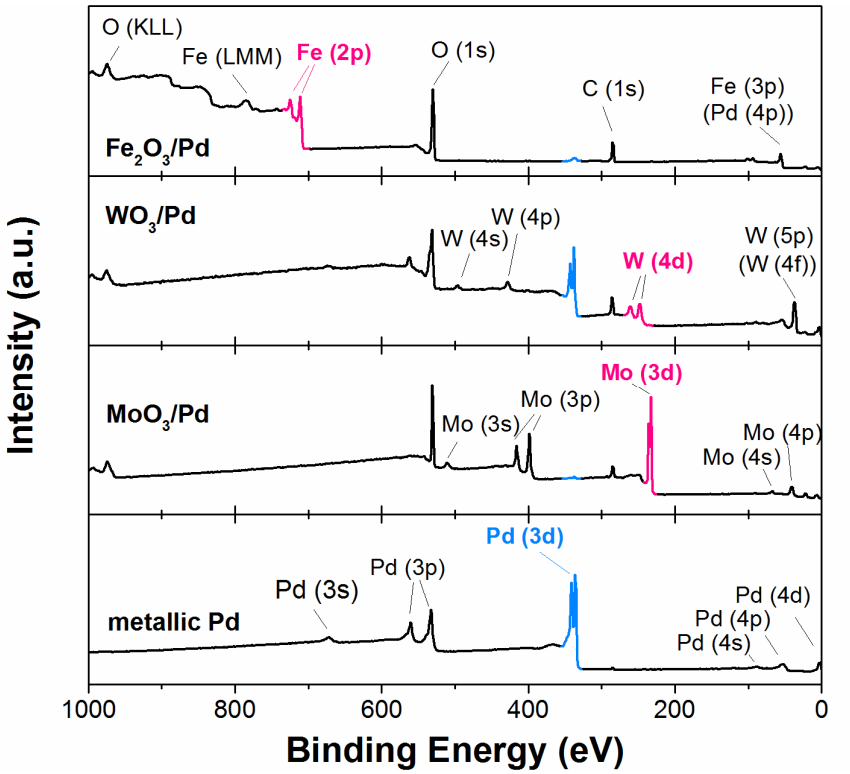

Figure S5. Survey XPS spectra of the metallic Pd plate and the as-prepared metal oxide/Pd catalysts.

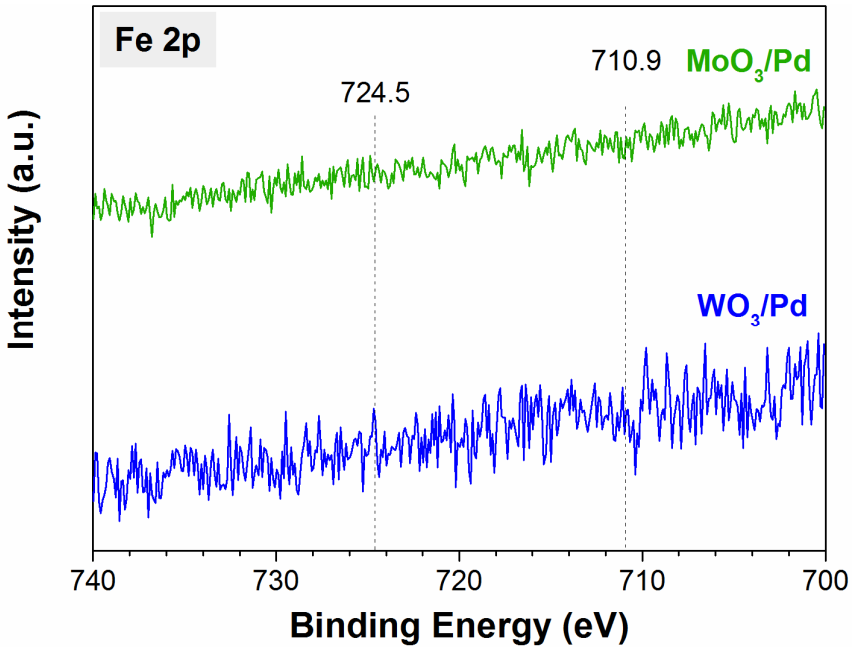

Figure S6. Core level XPS spectra of Fe 2p in the as-produced metal oxide/Pd catalysts.

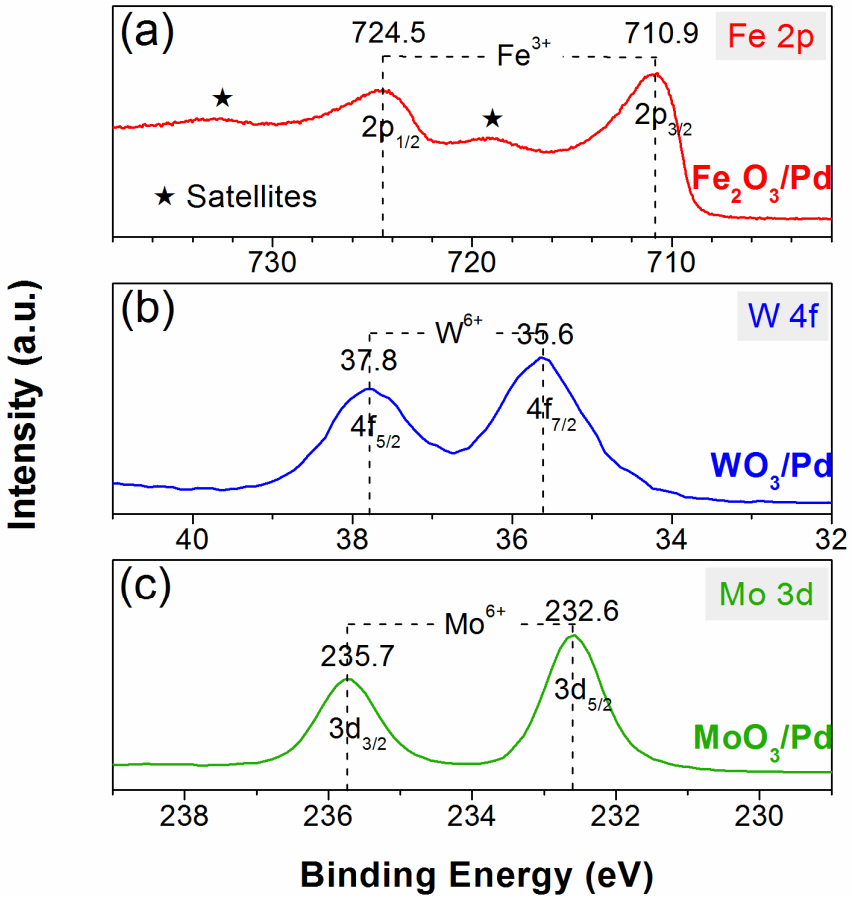

Figure S7. Core level XPS spectra of (a) Fe 2p in Fe_2O_3/Pd, (b) W 4f in WO_3/Pd, and (c) Mo 3d in MoO_3/Pd catalysts.

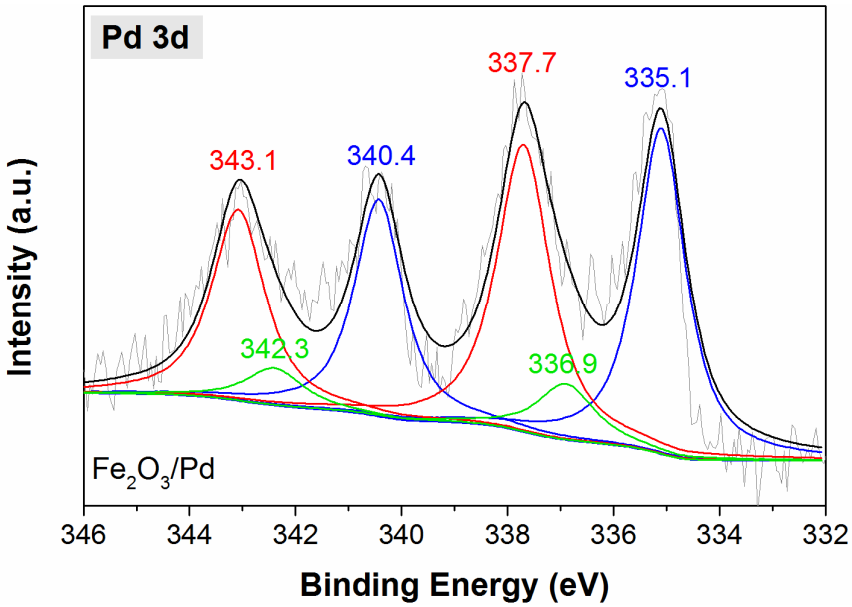

Figure S8. Deconvolution of the core level XPS spectra of Pd 3d in Fe_2O_3/Pd catalyst.

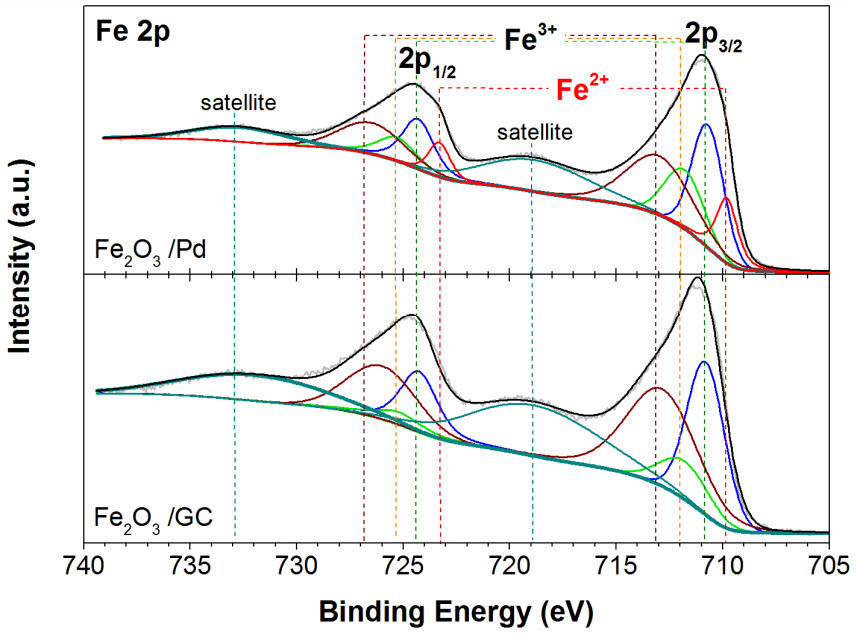

Figure S9. Deconvolution of the core level XPS spectra of Fe 2p in Fe_2O_3/Pd and Fe_2O_3/GC catalysts.

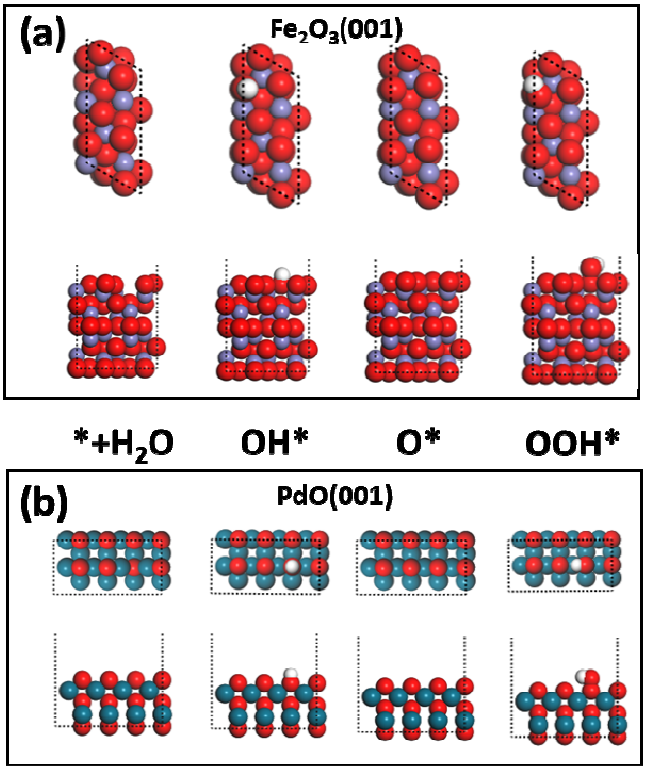

Figure S10. The top and side views of Fe_2O_3 (001) (panel a) and PdO (001) (panel b).

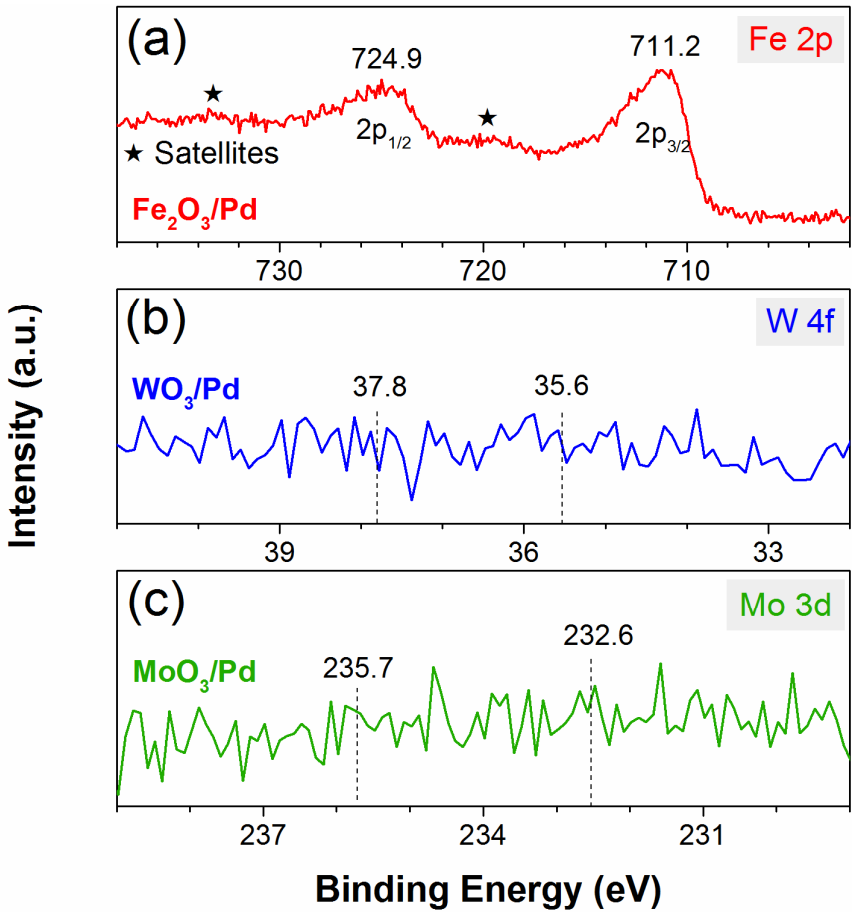

Figure S11. Core level XPS spectra of (a) Fe 2p in Fe_2O_3/Pd, (b) W 4f in WO_3/Pd, and (c) Mo 3d in MoO_3/Pd catalysts after the durability test.

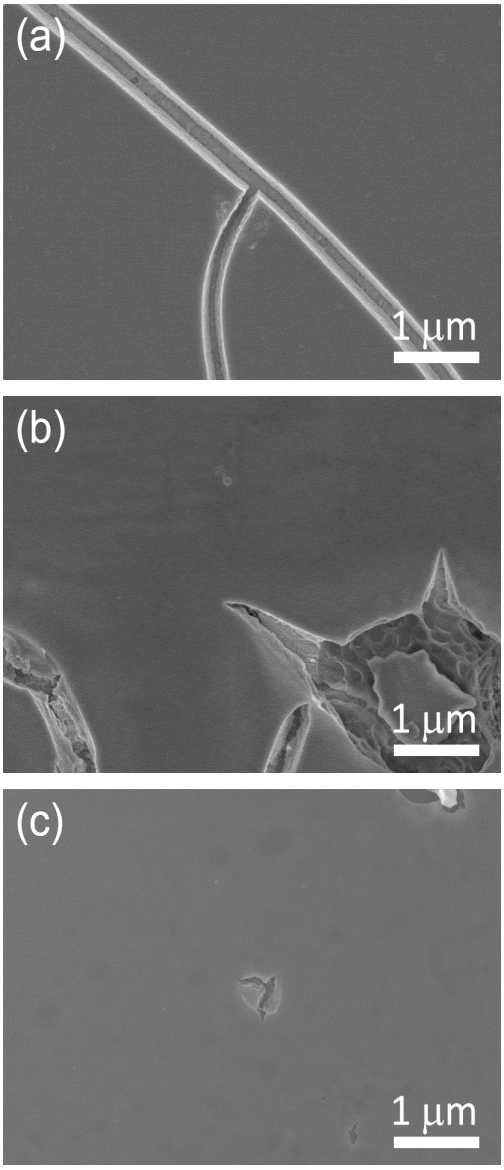

Figure S12. SEM images of the Fe_2O_3/Au (a), Fe_2O_3/Pt (b), and Fe_2O_3/GC (c) catalysts prepared with pyrolysis method.

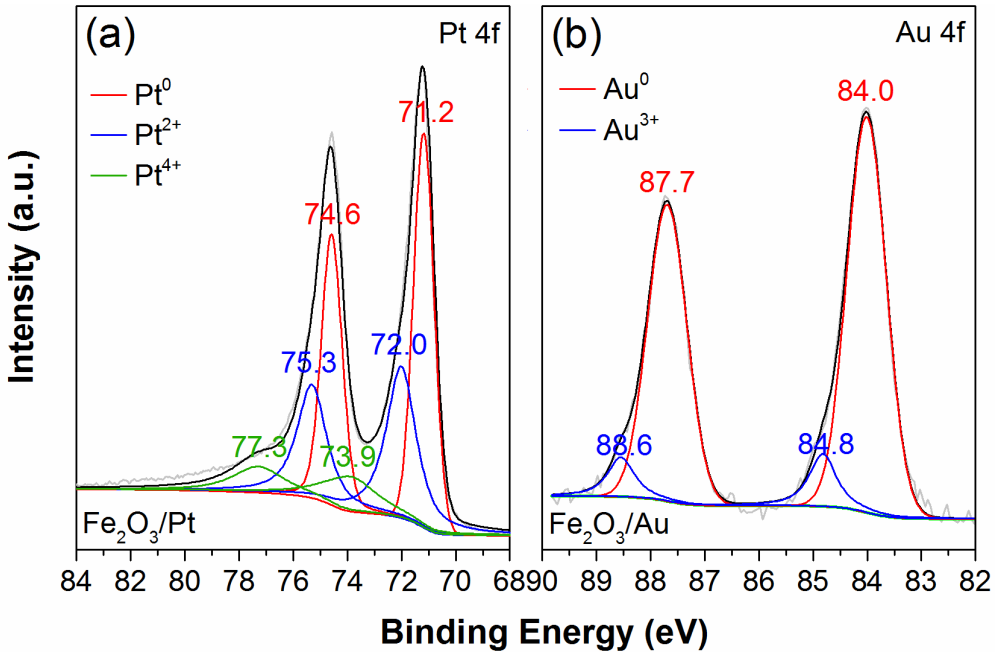

Figure S13. Deconvolution of the core level XPS spectra of (a) Pt 4f in Fe_2O_3/Pt and (b) Au 4f in Fe_2O_3/Au catalysts.

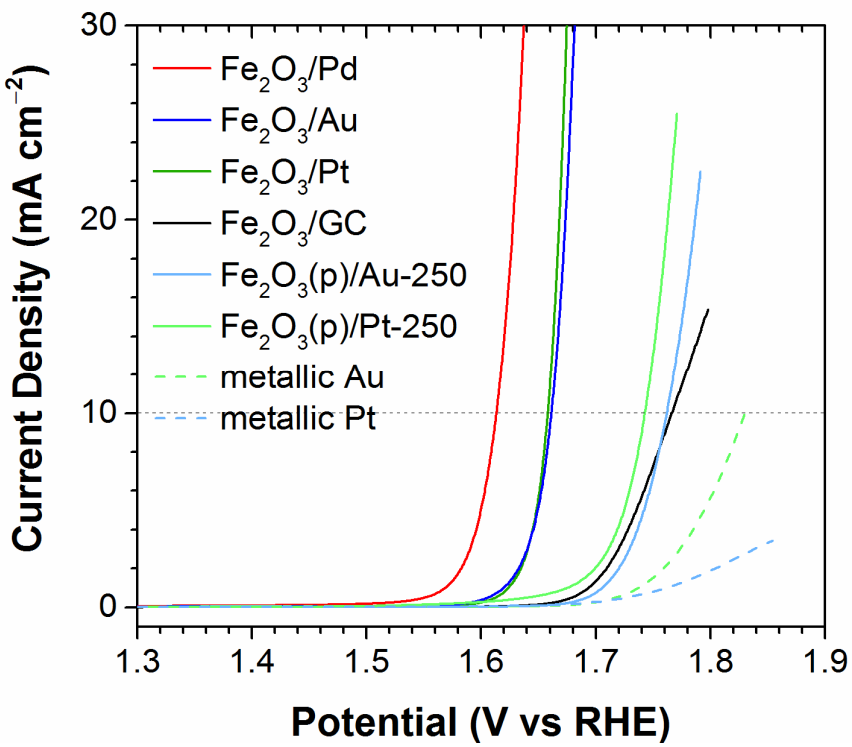

Figure S14. OER electrocatalysis in 1 M KOH. *iR*-corrected LSV curves recorded at a scan rate of 10 mV s^{-1} on metallic Au and Pt plates, and on Fe_2O_3/Pd, Fe_2O_3/Au, Fe_2O_3/Pt, Fe_2O_3/GC, Fe_2O_3(p)/Au-250, and Fe_2O_3(p)/Pt-250 samples.

3. Supporting Tables

Table S1. Catalysts Synthesis Parameters.

Catalysts	Annealed temperature (ºC)[a]	Precursors[b]
metallic Pd	–	–
Pd-250	250	–
Pd-350	350	–
Pd-450	450	–
Fe_2O_3/Pd	250	$Fe(NO_3)_3$
MoO_3/Pd	350	$(NH_4)_6Mo_7O_{24}$
WO_3/Pd	450	$(NH_4)_{10}H_2(W_2O_7)_6$
Fe_2O_3/GC	250	$Fe(NO_3)_3$
MoO_3/GC	350	$(NH_4)_6Mo_7O_{24}$
WO_3/GC	450	$(NH_4)_{10}H_2(W_2O_7)_6$
Fe_2O_3(p)/Pd	–	Fe_2O_3[c]
MoO_3(p)/Pd	–	MoO_3[c]
WO_3(p)/Pd	–	WO_3[c]
Fe_2O_3(p)/Pd-250	250	Fe_2O_3[c]
MoO_3(p)/Pd-350	350	MoO_3[c]
WO_3(p)/Pd-450	450	WO_3[c]
Fe_2O_3/Au	250	$Fe(NO_3)_3$
Fe_2O_3/Pt	250	$Fe(NO_3)_3$

[a]The precursor coatings are annealed directly under the corresponding temperatures in air for 1 hour. The pyrolysis temperatures are adopted according to the completely thermal decomposition of corresponding precursors.[S8-S10]

[b]Ten μL precursor aqueous solution with metal element concentration of 10 mM was pipetted onto each freshly cleaned metal plate.

[c]The powdery metal oxides were prepared by directly pyrolyzing the precursor reagent powders in air at the same temperature as producing corresponding metal-oxide/Pd catalysts.

Table S2. The ZPE entropy values used during the calculation. These values are taken from Ref. S5 and S7.

Species	TS (eV)	ZPE (eV)
H_2(g)	0.41	0.27
H_2O(g)[a]	0.67	0.59
O*	0	0.08
OOH*	0	0.47
OH*	0	0.15

[a]We used gas-phase H_2O at 0.035 bar as the reference state because at this pressure liquid water is equilibrium with gas-phase H_2O at 300 K.

Table S3. The metal element valences and the OER activities of the as-produced catalysts.

Catalysts	metal element valences [a]	η_{10} (mV)[b]	$j_{\eta = 400\ \mathrm{mV}}$ (mA cm^{-2})
Fe_2O_3/GC	Fe (+3)	540	0.075
Fe_2O_3/Au	Au (0, +3); Fe (+2, +3)	431	1.7
Fe_2O_3/Pt	Pt (0, +2, +4); Fe (+2, +3)	428	1.5
Fe_2O_3/Pd	Pd (0, +3); Fe (+2, +3)	383	16.0

[a] Characterized from the XPS spectra.

[b] Overpotential at j = 10 mA cm^{-2}.

References

(S1) Paolo, G.; Stefano, B.; Nicola, B.; Matteo, C.; Roberto, C.; Carlo, C.; Davide, C.; Guido, L. C.; Matteo, C.; Ismaila, D.; Andrea Dal, C.; Stefano de, G.; Stefano, F.; Guido, F.; Ralph, G.; Uwe, G.; Christos, G.; Anton, K.; Michele, L.; Layla, M.-S.; Nicola, M.; Francesco, M.; Riccardo, M.; Stefano, P.; Alfredo, P.; Lorenzo, P.; Carlo, S.; Sandro, S.; Gabriele, S.; Ari, P. S.; Alexander, S.; Paolo, U.; Renata, M. W. QUANTUM ESPRESSO: A Modular and Open-Source Software Project for Quantum Simulations of Materials. *J. Phys.: Condens. Mat.* **2009**, *21*, 395502.

(S2) Man, I. C.; Su, H. Y.; Calle‐Vallejo, F.; Hansen, H. A.; Martínez, J. I.; Inoglu, N. G.; Kitchin, J.; Jaramillo, T. F.; Nørskov, J. K.; Rossmeisl, J. Universality in Oxygen Evolution Electrocatalysis on Oxide Surfaces. *ChemCatChem* **2011**, *3*, 1159–1165.

(S3) Jones, R. O.; Gunnarsson, O. The Density Functional Formalism, Its Applications and Prospects. *Rev. Mod. Phys.* **1989**, *61*, 689–746.

(S4) Stefan, K.; P., P. J.; Peter, B. Molecular and Solid‐State Tests of Density Functional Approximations: LSD, GGAs, and meta‐GGAs. *Int. J. Quantum Chem.* **1999**, *75*, 889–909.

(S5) Nørskov, J. K.; Rossmeisl, J.; Logadottir, A.; Lindqvist, L.; Kitchin, J. R.; Bligaard, T.; Jónsson, H. Origin of the Overpotential for Oxygen Reduction at a Fuel-Cell Cathode. *J. Phys. Chem. B* **2004**, *108*, 17886–17892.

(S6) Hansen, H. A.; Rossmeisl, J.; Nørskov, J. K. Surface Pourbaix Diagrams and Oxygen Reduction Activity of Pt, Ag and Ni(111) Surfaces Studied by DFT. *Phys. Chem. Chem. Phys.* **2008**, *10*, 3722–3730.

(S7) Chen, J.; Fang, L.; Luo, S.; Liu, Y.; Chen, S. Electrocatalytic O2 Reduction on Pt: Multiple Roles of Oxygenated Adsorbates, Nature of Active Sites, and Origin of Overpotential. *J. Phys. Chem. C* **2017**, *121*, 6209–6217.

(S8) French, G. J.; Sale, F. R. A Re-investigation of the Thermal Decomposition of Ammonium Paratungstate. *J. Mater. Sci.* **1981**, *16*, 3427–3436.

(S9) Yuvaraj, S.; Fan-Yuan, L.; Tsong-Huei, C.; Chuin-Tih, Y. Thermal Decomposition of Metal Nitrates in Air and Hydrogen Environments. *J. Phys. Chem. B* **2003**, *107*, 1044–1047.

(S10) Kovács, T. N.; Hunyadi, D.; de Lucena, A. L. A.; Szilágyi, I. M. Thermal Decomposition of Ammonium Molybdates. *J. Therm. Anal. Calorim.* **2016**, *124*, 1013–1021.